Materials Science in Semiconductor Processing 83 (2018) 33–41

Contents lists available at ScienceDirect

Materials Science in Semiconductor Processing

journal homepage: www.elsevier.com/locate/mssp

Effects of interfacial layer-by-layer nanolayers on the stability of the Cu TSV: Diffusion barrier, adhesion, conformal coating, and mechanical property

Daekyun Jeong[a,1], Rahim Abdur[a,1], Young-Chang Joo[b], Jae-il Jang[c], Pil Ryung Cha[a], Jiyoung Kim[d], Kyeong-Sik Min[e], Jaegab Lee[a,*]

[a] School of Advanced Materials Engineering, Kookmin University, Seoul 02707, Republic of Korea
[b] Department of Materials Science & Engineering, Seoul National University, Seoul 08826, Republic of Korea
[c] Division of Materials Science & Engineering, Hanyang University, Seoul 04763, Republic of Korea
[d] Department of Materials Science & Engineering, The University of Texas at Dallas, TX 75080-3021, USA
[e] School of Electrical Engineering, Kookmin University, Seoul 02707, Republic of Korea

ARTICLE INFO

Keywords:
Through-Silicon Via (TSV)
Layer-by-layer (LbL)
Poly(allylamine) hydrochloride (PAH)/ polystyrene sulfonate (PSS)
Nano indentation
Stress reduction
Conformal coating

ABSTRACT

The Through-Silicon (Si) Via (TSV) is the integration technology for three-dimensional integrated-circuit packaging. The layer-by-layer (LbL) technique has been used to deposit flexible poly(allylamine) hydrochloride (PAH)/polystyrene sulfonate (PSS) multilayers inside scalloped Si trenches of a high aspect ratio, fabricated by the Bosch-etching process. An outstanding control of the thickness and the conformality of the polymer layers, along with a significantly improved planarization, was achieved due to the LbL-technique self-termination effects. In addition, the basic properties of the polymer layers have been characterized: diffusion-barrier properties, adhesion, density, and elastic modulus. The results of this study demonstrate the feasibility of LbL multilayers regarding the TSV liner for the vertical interconnect accesses with a high aspect ratio of highly scalloped surface walls.

1. Introduction

The three-dimensional (3D) integration of integrated circuits using Through-Silicon (Si) Via (TSV) technology has received attention because of the enhanced performance and functionality of the corresponding multilevel chip that is fabricated by the vertical stacking of a diversity of functional chips such as the complementary metal–oxide–semiconductor (CMOS), microelectromechanical systems (MEMS), and bio-chips [1–7]. Copper (Cu) has been widely used as a filling conductor in the TSV owing to its high conductivity and compatibility with back end of line (BEOL) processing and interconnects. In addition, the lower overall interconnection length and parasitic capacitance of the Cu-TSV chip interconnections lead to a significant reduction of the power consumption as well as a dramatic improvement of the compactness [2,8–11].

In terms of the 3D integration, however, Cu TSVs have represented a challenging technology, raising major reliability issues such as Cu protrusion, delamination at the Cu/dielectric interface [12–14], Cu contamination, and the leakage current [15–18]. The subjecting of the fabrication steps to various temperature cycles and the resultant thermal stress lead to protrusion and interfacial delamination in Cu TSVs [19,20]. In addition, the uniform coating of a thin diffusion barrier over the scalloped sidewall of TSVs that are produced by the Bosch process presents an additional difficulty [21–23], leading to a Cu-diffusion-induced degradation of the electrical performances [15,16]. The periodical sidewall roughness also acts as a stress concentrator [24], and this generates cracks and voids when the sidewall is subjected to thermal annealing at relatively high temperatures.

A number of reports on the relaxation of the thermomechanical stress that occurs due to the difference of the thermal-expansion coefficient between Cu and Si have been published; for example, with respect to the post annealing of Cu TSVs for the control of the plastic deformation and microstructure [12,25,26], and the trench-structure design [27,28]. In addition, the formation of a chemical vapor deposition (CVD) dielectric buffer layer in between the Cu TSV and the Si also reduces the thermal stress, as well as improving the Cu coverage over the scalloped sidewall. In the case of polymer dielectric buffer layers, additional advantages such as a low capacitance for the vertical interconnect accesses and simple and low-cost processes have been obtained [29–31]. Various polymer-deposition methods including spray

* Corresponding author.
E-mail address: lgab@kookmin.ac.kr (J. Lee).
[1] Authors contributed equally.

https://doi.org/10.1016/j.mssp.2018.04.008
Received 25 November 2017; Received in revised form 7 March 2018; Accepted 8 April 2018

coating [32], wet (solution) process [33], vacuum deposition [29], and spin coating [31,34,35] have been employed to provide the polymer filling of the Si annular trench that is fabricated by dry etching, or to achieve a conformal coating of the inside walls in the trenches and Vias [29,36].

It has been reported that the use of a soft polymer material as the TSV liner significantly reduces the capacitance and the current leakage of Cu TSVs [37], the thermally induced Si cracking, and the Via failure [38], demonstrating the feasibility of the TSV polymer dielectric layer. The filling of deep annular trenches with polymer, however, is challenging because of the tendency of air bubbles to become trapped at the trench bottom. In addition, the precise control of the thickness and the conformality with the application of polymer films is difficult to achieve, especially over the scalloped walls of high-aspect-ratio Vias [39,40].

The layer-by-layer (LBL) method provides an excellent control of the thickness due to its inherent self-termination capability [41,42]. In addition, a tailoring of the surface properties allows for the enhanced adhesion of Cu to the dielectrics and the immobilization of the Cu, leading to improved diffusion-barrier properties for Cu metallization [43,44]. Furthermore, it produces low-density polymer multilayers that can absorb the thermal stress that arises from the coefficient of thermal expansion (CTE) difference during the thermal cycling.

In this study, the employment of the LbL technique facilitated the achievement of the planarization of poly(allylamine) hydrochloride (PAH)/polystyrene sulfonate (PSS) multilayers over the scalloped sidewall of high-aspect-ratio (depth to width = 9:1) trenches that were fabricated by the Bosch-etching process, and a complete polymer coverage of the trenches. In addition, the material properties of the polymer nanofilms such as adhesion, barrier properties, and elastic modulus were investigated to determine the feasibility of the LbL multilayers that are produced by the simple and low-cost LbL technique for TSV liners.

2. Experimental

LbL bilayers are deposited by using the following two different types of electrolyte: positively charged PAH (Sigma-Aldrich, U.S.A.) and negatively charged PSS (Sigma-Aldrich, U.S.A.). These can be alternately coated on the surface to form the as-designed multilayer. To form the LbL multilayers on the Si substrate, a solution-dipping method was used with 0.2-M PAH and sodium hydroxide (NaOH) with a pH of 9 and 0.2-M PSS and sodium chloride (NaCl) with a pH of 5. The Si substrate was cleaned by a dipping in piranha solution for 10 min, followed by its exposure to ultraviolet (UV) to negatively charge the substrate. The LbL assembly for which the alternate dipping into the 0.2-M aqueous solutions containing the polyelectrolytes (PEs) was undertaken was carried out [41,45–49]. The repeating of the process enabled the formation of the as-designed multilayers. In addition to the coating on the planar Si surface, the conformal deposition of the LbL multilayers was investigated over the deep Si trench that was fabricated by the Bosch process using a deep reactive ion etcher (DRIE). The width and the depth of the Si trench are 5 μm and 45 μm, respectively.

For the measurement of the elastic modulus of the LbL multilayers by the depth-sensing nanoindentation method, LbL multilayers of different thicknesses (70, 140, and 250 nm) were deposited on poly(dimethylsiloxane) (PDMS) substrates of a thickness of approximately 5 mm. The PDMS samples were prepared by a complete mixing of the Sylgard 184 elastomer base and a curing agent (Dow Corning Corporation, U.S.A.) with a 10:1 base/agent mass ratio, and this was followed by pouring the mixture into a petri dish and degassing it in air for 1 h to remove the air bubbles. Then the 10:1 PDMS was cured in an oven for 1 h at 70 °C. All of the indents were performed using the TI-950 TriboIndenter (Hysitron, Inc., U.S.A.) equipped with an XZ displacement stage. A flat punch-tip geometry, which was commercially available (Hysitron, Inc., U.S.A.), with a diameter of 21.2 μm and a 90° diamond-cone shape was used for the testing.

All of the indents fully captured the force curves using a displacement-controlled load function that detected the surface, with a setpoint of 2 μN to prevent a false surface detection during the testing; they were then loaded to the target displacement (500, 1000, and 2000 nm) at a rate of 100 nm/s, held at the peak displacement for 1 s, and were finally unloaded at a rate of 100 nm/s until they were beyond the contact of the sample. The peak applied displacement varied from 500 to 1000 nm, and it also reached 2000 nm. The datasets were manually zeroed to the point where the load commenced its monotonic increase prior to the modulus calculation.

For the flat-punch analysis, it was assumed that the indenter would behave equivalently to a cylindrical flat punch with a constant contact area $A = \pi \quad r^2$, where r is the cone radius. The unloading stiffness (S), the slope of the upper portion of the unloading curve, for each indent was determined by fitting a power law to the initial 80–95% of the unloading-curve data using the Hysitron software (Hysitron, Inc., U.S.A.). The reduced modulus was calculated using the Oliver–Pharr method [50], as follows:

$$E_r = \frac{\sqrt{\pi}}{2}\frac{s}{\sqrt{A}} = \frac{s}{2r}. \quad (1)$$

In addition, the reduced modulus, E_r, can be expressed in terms of the elastic properties of the indenter and the specimen, as follows:

$$\frac{1}{E_r} = \frac{(1-\quad \nu_i^2)}{E_i} + \frac{(1-\quad \nu_f^2)}{E_f}, \quad (2)$$

where E and ν are the elastic modulus and Poisson's ratio for the specimen, and E_i and ν_i are the same parameters for the indenter. For the soft materials that were indented by the stiff tip, the material E is related to the reduced modulus by

$$E = (1 - \nu^2)E_r, \quad (3)$$

where ν is the material Poisson's ratio, and the ν of the PDMS and LbL multilayers was considered as 0.5 [51].

The thickness, coverage, and morphology of the nanolayered structures that were deposited on the planar Si-wafer surface and the scalloped TSV pattern were measured using the JEOL-7401F (Japan) field-emission scanning electron microscopy (FESEM). A quartz-crystal microbalance (QCM) was used to measure the change in the mass of the material that was deposited after each adsorption step. The water contact angle of the self-assembled films was measured using the Phoenix 300 instrument (Surface Electro Optics, South Korea). In addition, a 2-MV Pelletron accelerator with a 2 MeV alpha particle and a 170° scattering angle was used to perform Rutherford backscattering spectroscopy (RBS) for the measurement of the compositional depth profile and the thickness of each layer. Furthermore, the sheet resistance was measured using a four-point probe (Chang Min Co. Ltd., Korea).

3. Results and discussion

3.1. Coating of the LbL multilayers and the conformal coating on the Si-trench sidewall

A dipping method was used to produce PAH/PSS-multilayer thin films on the silicon dioxide (SiO_2)-coated Si wafers. The two different types of PE polymers are the weak and the strong PEs; weak PEs such as PAH and polyacrylic acid (PAA) carry charge densities that are tunable by pH adjustments, while strong PEs such as PSS have a surface charge density that is independent of the pH of the aqueous solution [41,52–54]. The pH values of the PAH and PSS dipping solutions are 9.0 and 5.0, respectively. A high PAH-solution pH increases the protonation of the PAH ammonium groups, thereby leading to an increase of the PAH surface charge density, while the adsorption of the PSS layer

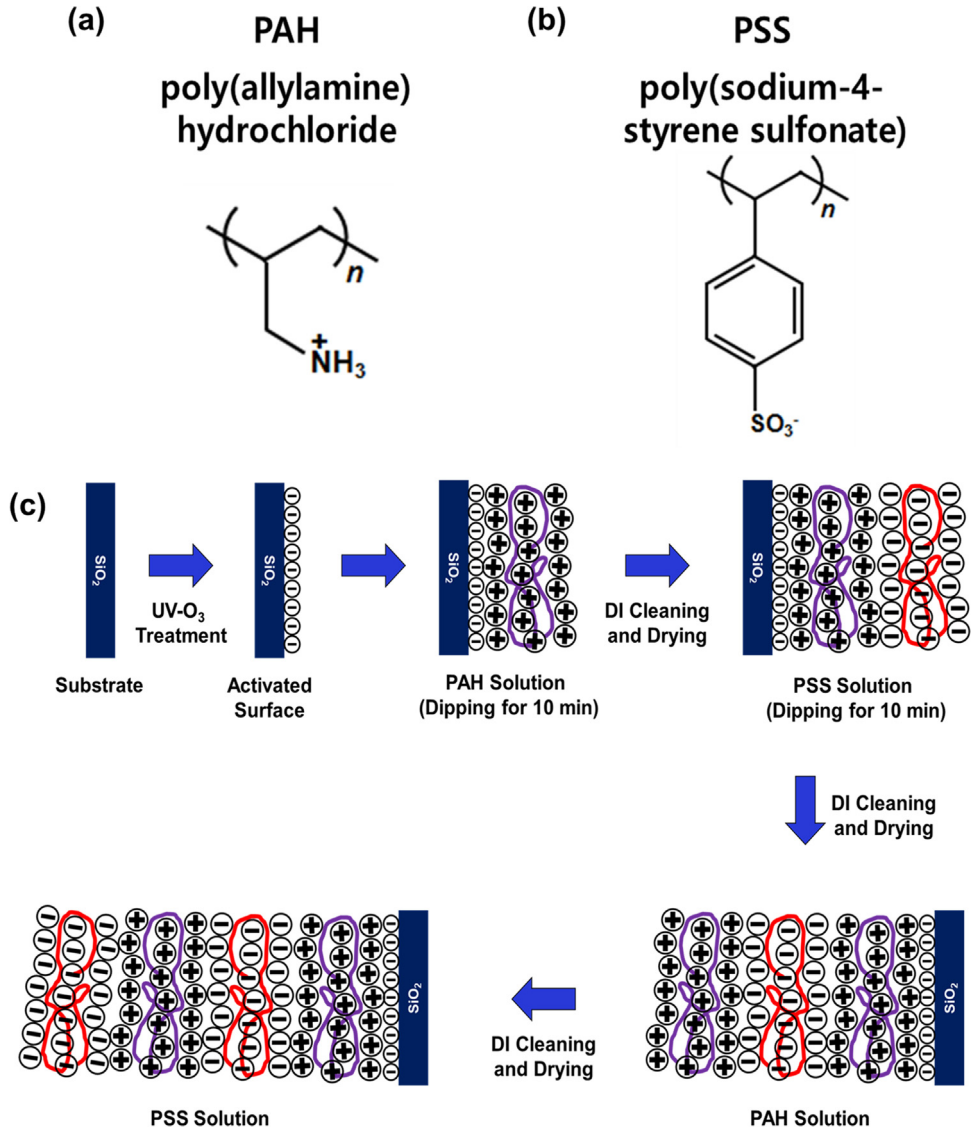

Fig. 1. The chemical structure of (a) poly(allylamine) hydrochloride and (b) poly(sodium-4-styrene sulfonate), and (c) the schematic of the process sequence of LBL assembly.

is independent of the pH of the PSS solution. Fig. 1 shows the chemical structure of PAH and PSS, and the schematic of process sequence of the typical LbL assembly [55], where 10-min adsorption intervals were used in this study since this was adequate in the proposed system.

To monitor the proper assembly, the QCM was used to measure the mass change of each deposited PE on the QCM electrode. The adsorbed mass Δm_A of the PEs was calculated from the change of the QCM frequency ΔF according to the Sauerbrey equation [56,57], as follows:

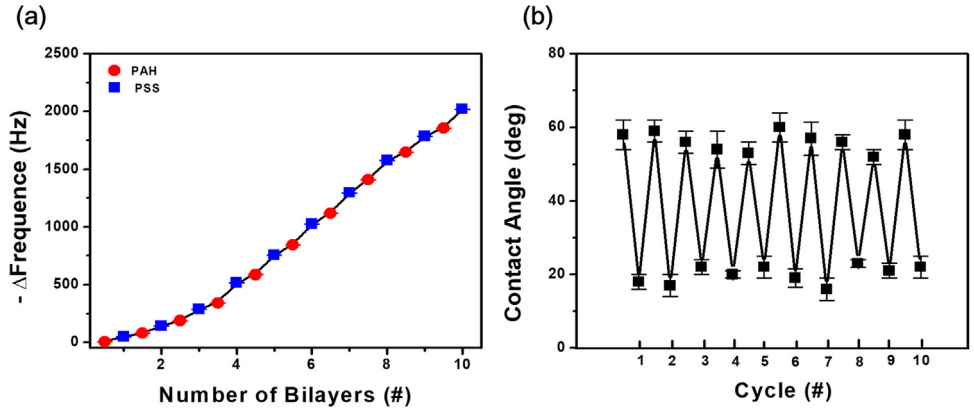

Fig. 2. (a) Frequency change of a quartz crystal oscillator and the corresponding change in adsorbed mass as a function of the number of PAH/PSS bilayers, and (b) the variation of water contact angles of the self-assembled $(PAH/PSS)_n$ films with the number of cycles.

$$\Delta m_A(\text{ng}) = -17.85 \times \Delta F(Hz). \quad (4)$$

In the proposed system with a Stanford Research Systems 5-MHz resonator (U.S.A.), a 1-Hz frequency decrease corresponds to a mass increase of 17.85 ng. The density of the LbL multilayers was calculated as 1.1 ± 0.1 g/cm^3 based on the mass changes of the frequency and the corresponding FESEM-measured thickness.

Fig. 2(a) shows the QCM-frequency shifts during the alternating adsorption of the PAH and PSS PEs. A regular film growth was observed after the bilayer adsorption was repeated approximately twice, indicating that the LbL multilayer films consisting of the anionic PSS and the cationic PAH were properly assembled, and comprised specific amounts of the PSS and the PAH that were alternatively adsorbed on the surface with the increasing of the deposition-layer number.

The water contact angles of the self-assembled $(PAH/PSS)_n$ films varied periodically, with spans of 18–22° for the PSS and 53–58° for the PAH, when the surface-adsorbed top layer was changed from the PSS to the PAH, as shown in Fig. 2(b), which are similar to the values in the report of Marta et al. [49]. The relatively low scatter of the contact-angle values that was measured on a given-layer surface indicates a homogeneous multilayer surface. In addition, the amplitude of the contact-angle variations represents the ionic strength between the oppositely charged PE layers, where a relatively high amplitude value implies a minor interpenetration of the PSS–PAH layers during their deposition.

3.2. Step coverage and degree of planarization

The Bosch-etching process provides a high-selectivity and high-aspect-ratio etching for Si as a result of repeated alternating isotropic-etching and sidewall-passivation processes [15,57]. The alternating etching mechanism, however, results in a scalloped sidewall of the Si trench, as shown in Fig. 3, which significantly degrades the reliability of Cu TSVs. LbL technology is a thin-film deposition method wherein the oppositely charged electrolytes alternately self-assemble on the surface via an electrostatic attraction in a self-terminating manner. This leads to a precise control of the thickness, a homogeneous and uniform coating of the LbL multilayers, and a capability that can improve such roughness and the step coverage of the deep Si trench. The LbL nanolayers were coated over the deep Si trench (width = 5 μm, depth = 45 μm) to investigate their effects on the multilayer coverage. To qualitatively estimate the ability of the LbL method regarding the coverage, both the step coverage and the planarization degree were measured as a function of the number of cycles. Fig. 4 shows a scanning electron microscope (SEM) image of the nanolayers that were coated on the deep Si trench with a thickness of approximately 165 ± 4.3 nm. The inset shows the coating of the LbL multilayers on the top, middle, and bottom regions, revealing a step coverage of more than 95%.

Fig. 5 shows the evolution of the coverage of the LbL multilayers on the scalloped sidewall with the number of bilayers. Very serious scalloping with sharp etch profiles can be observed on the Bosch-etched sidewall of the Si trench, which was significantly improved with the coating of the LbL multilayers. In addition, the degree of planarization that was defined as $(1- R_f/R_i) \times 100$—where R_f is the rms (root mean square) of the roughness of the LbL-multilayer coated surface, and R_i is the rms of the initial roughness of the etched-Si surface—was increased by up to 70% as the LbL thickness was increased to 165 nm. The rms value Ri is the square root of the arithmetic mean of the squares of distance between the etched Si surface and the top flat surface, and Rf is the rms value of the distance between the LBL multilayers-coated Si surface and the top flat surface.

3.3. Adhesion of the LbL films to Cu and Si, and their barrier properties against Cu

Self-assembled molecular Nanolayers (MNLs) are able to tailor interfacial properties with molecular terminal groups. Such terminal groups including –SH [58], $–NH_2$ [59], –COOH [59], and $–SO_3$ [60] chemically bind to Cu to suppress its interfacial diffusion, and also, the organosilanes (-$SiOCl_3$, -$SiORe_3$) of the MNLs react with the hydroxylated SiO_2 to form the strong siloxane bridging of Si–oxygen (O)–Si. These characteristics provide an excellent diffusion-barrier ability and Cu-metallization adhesive properties. Gandhi demonstrated the use of PAH–PSS bilayers in the effective blockage of the Cu transportation into silica that involves a strong bonding of the PAH PE to SiO_2 [44].

In the present study, the polymer bilayers of the PSS and PAH PEs were coated on the hydroxylated-Si surface that was produced by the UV exposure, and the newly coated surface was then investigated regarding the ability of the polymer multilayers to adhere to Cu and Si, as well as their barrier ability against the Cu transportation. Adhesive-tape

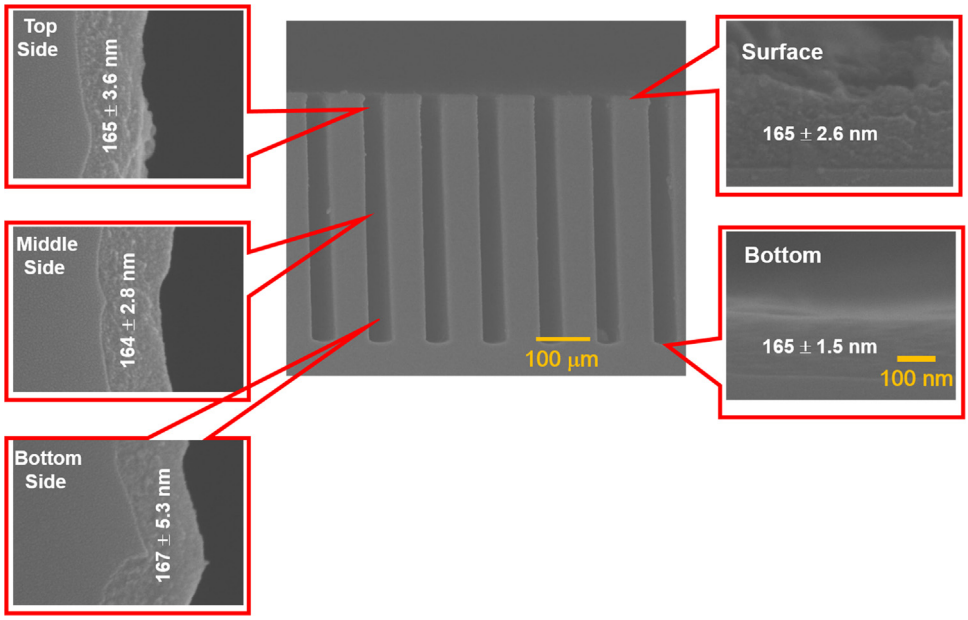

Fig. 3. SEM image of LbL multilayers coated on the deep trench of Si. The inset shows the coating of LbL multilayers on three regions (surface, bottom, and sidewall (top, middle, and bottom) of Si trench), revealing more than 95% of step coverage.

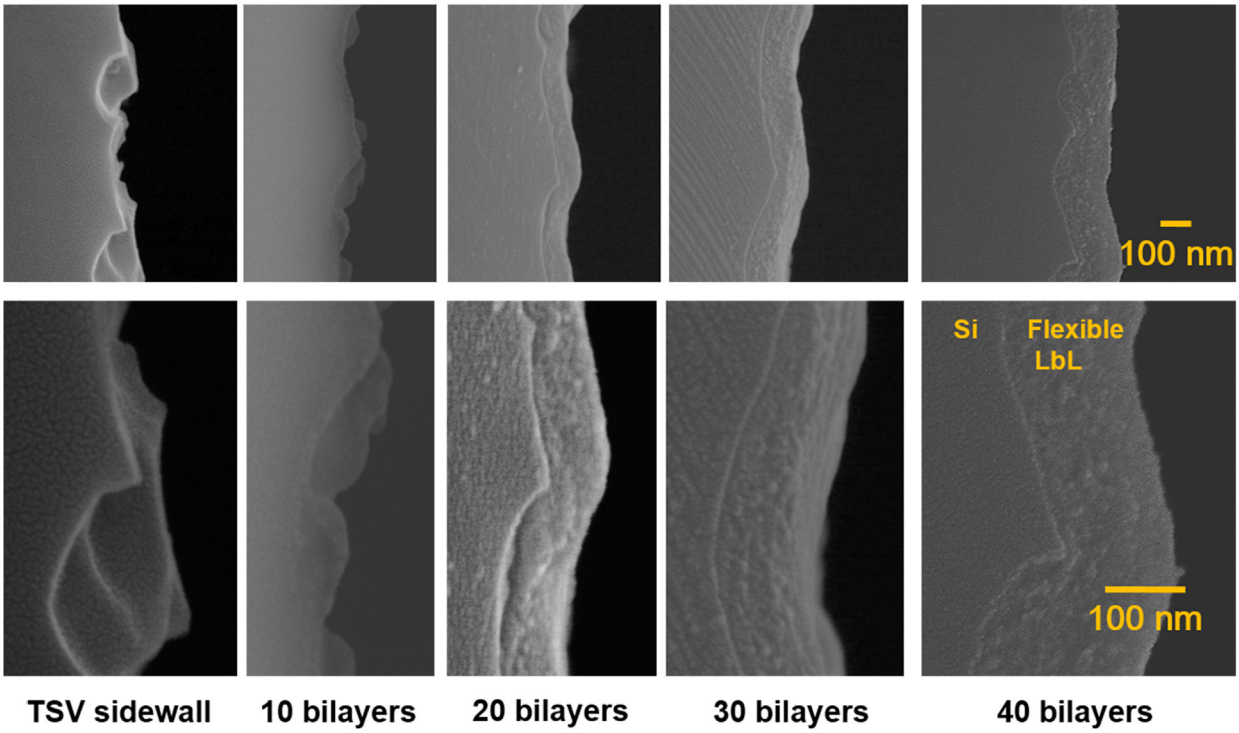

Fig. 4. Coverage of LbL multilayers coated at various number of bilayers over the scalloped Si sidewall.

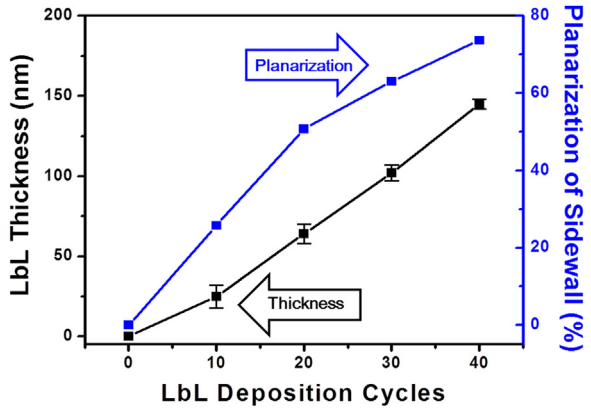

Fig. 5. The thickness of LbL multilayers and the corresponding planarization as a function of LbL deposition cycles.

testing [61] was performed on the Cu/LbL-multilayer/Si samples, thereby revealing a strong adhesion between Cu, the PSS/PAH multilayers, and Si when Cu was deposited on more than three bilayers of the PE-coated Si, as shown in Fig. 6. A single PSS/PAH bilayer is insufficient for the holding of the Cu film, and this is probably due to the insufficient surface density of the bilayer $-SO_3^-$ groups. The strong adhesive actions of Cu to PSS and of PAH to Si are due to the binding of the Cu to the SO_3^- in PSS and the nitrogen (N)–Si bonding that is a result of the reaction between the NH_3^+ and OH^- groups, respectively.

The diffusion-barrier properties for Cu metallization have been characterized by a measurement of the sheet resistance of Cu in the Cu/LbL layers with the (PAH/PSS)*n*/Si (n = 1, 3, 5) structure that was annealed at various annealing temperatures, and also by using RBS.

Fig. 7(a) shows the schematic of sample structure to measure the sheet resistance of Cu deposited LbL layer coated Si substrates and Fig. 7(b) shows the variation of the Cu sheet resistance as functions of the temperature and the number of bilayers. The Cu/Si structure was annealed to reveal that the onset temperature T_{on}, at which the sheet resistance started to increase, is approximately 250 °C; in contrast, the Cu/$(PSS/PAH)_n$/Si (n = 1, 3, 5) structure showed a drastic increase of the T_{on}. The single PSS–PAH bilayer increased the T_{on} from 250 °C to approximately 500 °C, effectively preventing the transportation of the Cu across the interface. In addition, the increasing of the number of bilayers from 1 to 3 (or 5) further increased the T_{on} up to approximately 550 °C. The significant increase of the diffusion-barrier property with the single bilayer, the thickness of which is 2.5 ± 0.5 nm, is due to a strong interfacial bond between the Cu and the surface functional groups such as SO_3^- [60]; furthermore, the additional increase of the resistance to the Cu diffusion in the $(PAH/PSS)_{3(or\ 5)}$ could be partly due to the improved bilayer coverage compared with that of the single bilayer, as well as the possibility that it is partly due to its interaction with the electrically charged electrostatic layers. Therefore, RBS was used to investigate the Cu diffusion through the LbL nanofilms during

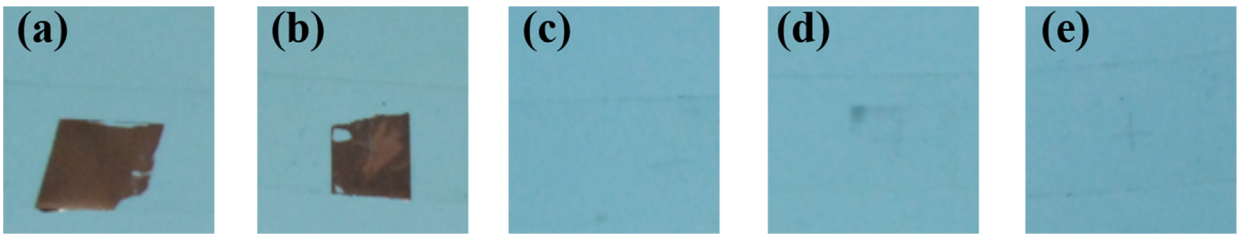

Fig. 6. Adhesion tape testing of (a) Cu/Si and Cu/(PAH/PSS)n/Si structures, where n equals (b) 1, (c) 3, (d) 5, and (e) 10.

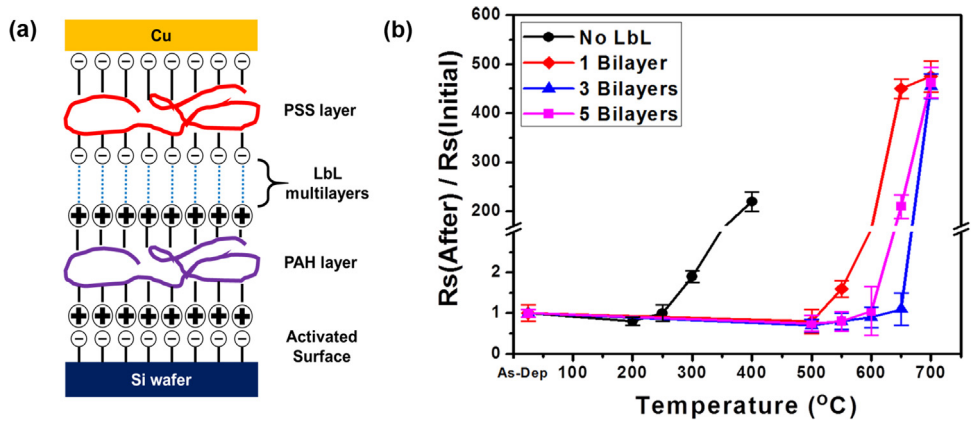

Fig. 7. (a) The schematic diagram of Cu films on LbL multilayer-coated Si substrates and (b) variation of sheet resistance as functions of annealing temperature and number of bilayers.

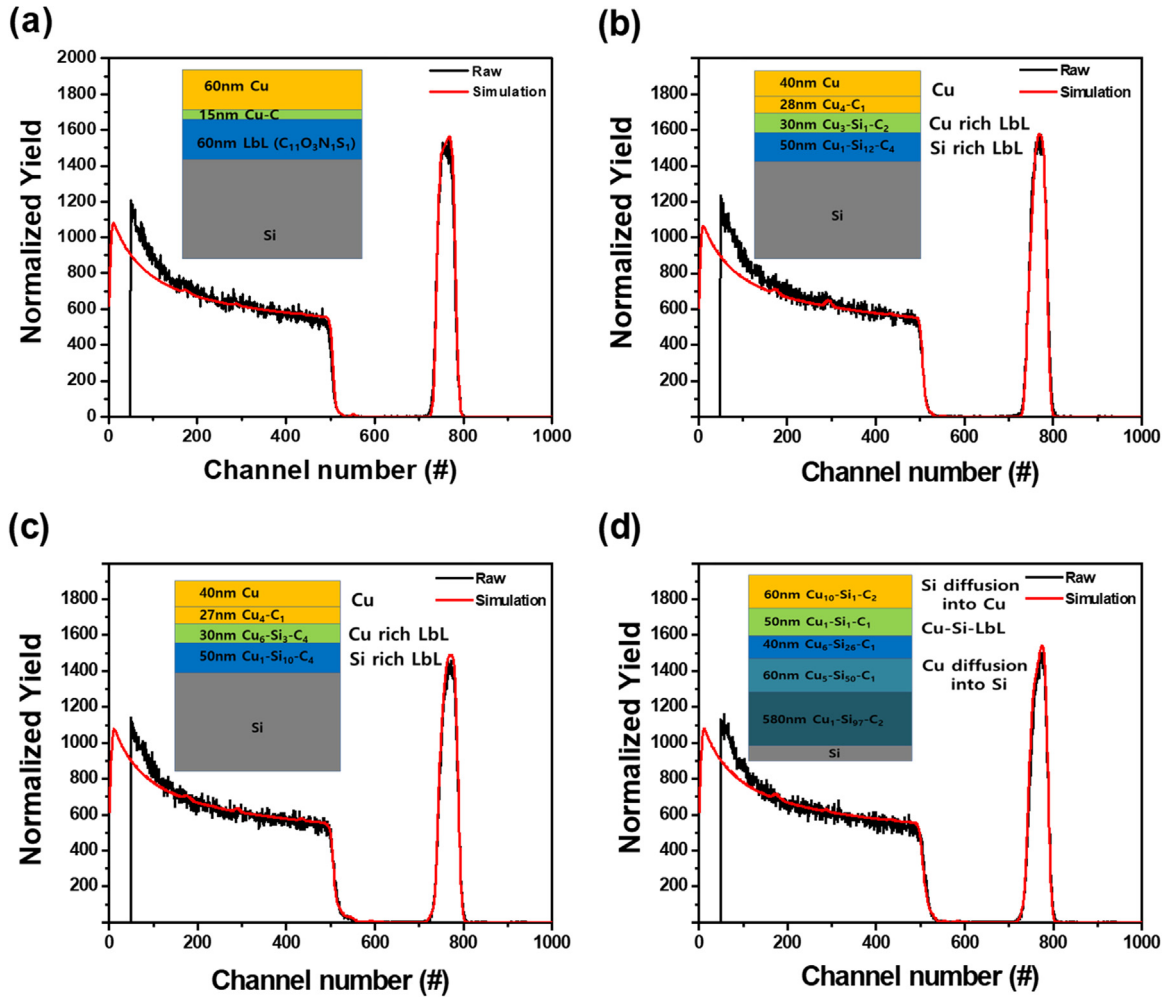

Fig. 8. RBS spectra of Cu/LbL multilayers $(PAH/PSS)_{10}$/Si substrate at various annealing temperatures (a) As deposited, (b) 500 °C, (c) 600 °C, and (d) 700 °C.

the annealing of the samples.

Fig. 8 shows the RBS spectra of the as-deposited and as-annealed Cu/LbL $(PSS/PAH)_{10}$/Si structures that were annealed at 500–700 °C for 30 min, and the Rump simulation was performed to reveal the layered structures that were formed as a result of the diffusion of Cu and Si into the LbL nanofilms. The composition of the PSS/PAH bilayers was considered as $C_{11}O_3N_1S_1$ in the simulation of the LbL multilayers. The simulation shows that the as-deposited structure consists of Cu (60 nm)/Cu–carbon (10 nm)/LbL (60 nm)/Si. At 500 °C, the Cu and Si were diffused into the LbL nanofilms to form the two-layered LbL film, the Cu-rich LbL (approximately 35 nm), and the Si-rich LbL (approximately 50 nm), as shown in the inset of Fig. 8. This led to an increase of the thickness of the LbL nanofilm compared with the 60-nm-thick LbL in the as-deposited films, and this is due to the interdiffusion of the Cu and the Si in the LbL nanofilms. The Cu and Si can be interdiffused and captured [62] between the oppositely charged PE layers in the form of nanoparticles, [63]. These charged PE bilayered structures immobilized the diffused Cu and Si, leading to additional improvements of the

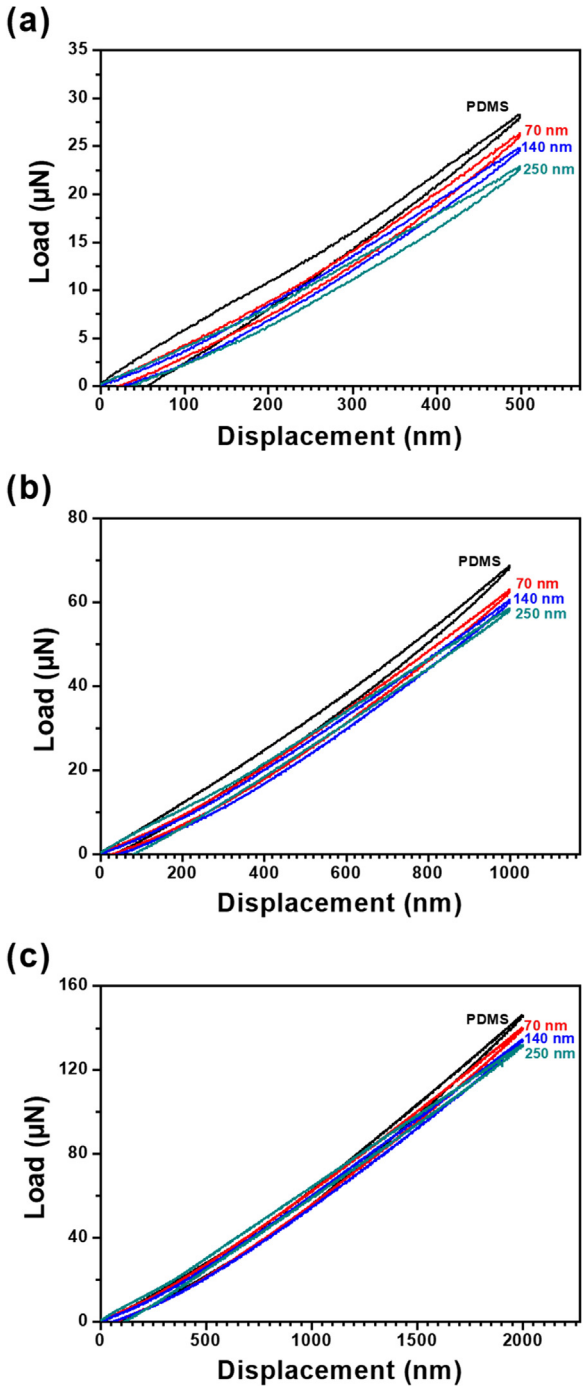

Fig. 9. Typical load-displacement curves obtained by indenting PDMS and different thickness of LbL nanofilms on PDMS to (a) 500 nm, (b) 100 nm, and (c) 200 nm of indentation displacement with a cylindrical flat tip.

diffusion barrier properties. A further increase of the temperature to 600 °C showed a similar feature of the bilayered structure in the LbL multilayers. The LbL nanofilms at 700 °C, however, failed as a result of the severe interdiffusion of the Cu and Si across the LbL nanofilms. These results are consistent with the sheet-resistance variation with the temperature.

3.4. Mechanical properties of the LbL nanolayers

3.4.1. Flat-punch nanoindentation (PDMS, LbL-coated PDMS)

The determination of the mechanical properties of thin films, especially very soft materials such as polymer, on a substrate using nanoindention has been difficult; in part, this is because of the influence of the substrate on the measured properties [64–66], and it is also due to the relatively sticky and viscous properties of polymers [67]. The effects of the substrate on the measurement of the thin-film properties increases as the film thickness decreases, and the elastic mismatch between the film and the substrate increases, leading to the inaccuracy of the measurement. Furthermore, the polymer-related material issues such as interfacial adhesion and viscoelasticity make it quite challenging to determine the contact area of the indenter tip, which the elastic-modulus calculation is based on [67]. In general, the indentation-based measurement of polymer thin films has employed the flat end tip since it allows for an accurate determination of the contact area during the indentation for which it remains constant. Therefore, a cylindrical-shape flat punch tip with a flat end was used to measure the elastic-modulus values of the PDMS and LbL nanofilms. To reduce the substrate effects on the measurement of the LbL nanofilms, a low-modulus PDMS was used as a substrate on which different-thickness LbL nanofilms were deposited.

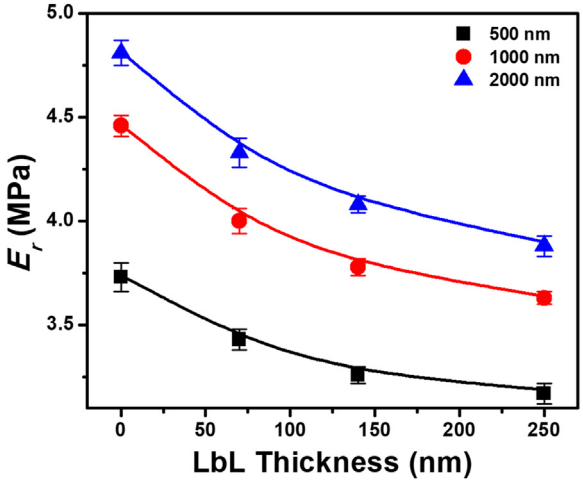

Fig. 10. The reduced elastic modulus of the LbL nanofilm-coated PDMS was plotted as a function of LbL film thickness at various (500 nm, 1000 nm, 2000 nm) displacement of nano indentation. Each curve was fitted by Eq. (5) with the α values corresponding to the thickness of LbL film (solid line and points indicate simulated data and experimental values respectively).

A series of indentations were made on 5-mm PDMS samples, as well as samples of other thicknesses (70, 140, and 250 nm), of the LbL multilayer-coated PDMS samples, with depths ranging from 500 to 2000 nm, to determine the elastic-modulus values of the PDMS and the LbL multilayers.

Fig. 9 shows typical load-displacement curves that were obtained from the indentation of the PDMS and different LbL nanofilm thicknesses on the PDMS using indentation displacements of (a) 500 nm, (b) 100 nm, and (c) 200 nm with a cylindrical flat tip. Based on these results, the stiffness values of the PDMS and the LbL nanofilm-coated PDMS were measured.

With the reduced elastic modulus of the PDMS sample that was calculated using Eq. (1), the mechanical properties of the diamond tip (Young's modulus of 1141 GPa, Poisson ratio of 0.07), and the contact area of the flat tip ($\pi r^2 \fallingdotseq 352.989\,\mu m^2$), it was then possible to calculate the elastic modulus of 3.43 MPa (average of 5 samples) for the PDMS using Eq. (2), which is close to the reported PDMS elastic modulus (3.79 ± 0.02 MPa) [68]. This finding supports the feasibility of this measurement technique for the measurement of the elastic modulus of such low-modulus polymer materials.

The reduced elastic modulus of the LbL nanofilm-coated PDMS was calculated using Eq. (1) and plotted as functions of the nanoindentation displacement and the LbL thickness, as shown in Fig. 10. The slight E_r

increase of the LbL-nanofilm-coated PDMS with the increasing of the indentation displacement and the decreasing of the LbL thickness is due to the increasing PDMS effects on the total elastic modulus.

To extract the elastic modulus of only the LBL nanofilm from the coated LbL nanofilm on the PDMS, the King's model [69], which includes the influence of the substrate compliance on the reduced modulus of film/substrate systems, was utilized as follows:

$$\frac{1}{E_r} = \frac{1-\nu_i^2}{E_i} + \frac{1-\nu_f^2}{E_f}\left(1-e^{-\frac{\alpha t}{a}}\right) + \frac{1-\nu_s^2}{E_s}\left(e^{-\frac{\alpha t}{a}}\right), \quad (5)$$

where a is the square root of the projected contact area of the diamond tip ($a = \sqrt{\pi r^2}$), t is the thickness of the film below the punch, and α is a numerically determined scaling parameter that is a function of a/t, the normalized punch size.

As the α is a strong function of the LbL thickness, an attempt was made to fit Eq. (5) to the E_f-displacement curve at a constant LbL thickness to obtain the α value corresponding to each of the thicknesses of the LbL nanofilms. The obtained α values are 2.562, 1.876, and 1.368 for the LbL thicknesses of 70, 140, and 250 nm, respectively, and the obtained E_f values are from 0254 to 0.251 MPa. With those α and E_f values, it became possible to properly fit Eq. (5) to the E_r–LbL thickness curve, as shown in Fig. 10. It is also noted that the elastic modulus of the LbL nanofilms is sufficiently low to relax the thermal stress that is induced by the difference in the thermal-expansion coefficient between Cu and Si.

4. Conclusion

This paper reports on the feasibility of the application of LbL multilayers as both a diffusion barrier and a dielectric buffer layer for the TSV. The use of the LbL technique provided an excellent conformal coating of the PAS/PSS multilayers over the high-aspect-ratio trenches and the achievement of the planarization on the scalloped etch profiles that were fabricated using the Bosch-etching process. In the Cu/LbL/Si stacks with the LbL comprising electrostatic bilayers, a strong bonding at the Cu–LbL interface inhibited the Cu transportation across the interface, and it is expected that an additional suppression of the Cu transportation through the LbL layers would occur due to the capturing of the Cu between the electrostatic bilayers. In addition, the chemical bonding of Cu–SO_3^- at the Cu–LBL interface and of Si-NH_3+ at the LbL–Si interface leads to a strong adhesion between Cu and Si. Furthermore, the nano indentation technique revealed a very low LbL-multilayer elastic modulus, so these multilayers can serve as a polymer buffer layer to reduce the thermally induced stress on Cu TSVs from the post annealing treatment. Consequently, the use of the LbL technique provides a low-cost, simple, and reliable Cu-TSV structure.

Acknowledgments

This study was supported by the Leading Foreign Research Institute Recruitment Program through the National Research Foundation of Korea (NRF) funded by the Ministry of Science, ICT and Future Planning (2013K1A4A3055679). This study was also supported by a National Research Foundation of Korea (NRF) Grant (No. 2015R1A5A7037615) funded by the Korean Government (MSIP) and Technology Innovation Program (Industrial Strategic Technology Development Program, 10035430, Development of reliable fine-pitch metallization technology) funded by the Ministry of Knowledge Economy (MKE, Korea).

References

[1] Interconnect, The International Technology Roadmap for Semiconductors, 2013. ⟨http://www.itrs2. net/itrs-reports.html⟩.
[2] S.F. Al-sarawi, D. Abbott, P.D. Franzon, A review of 3-D packaging technology, IEEE Trans. Compon. Pack. B 21 (1998) 2–14.
[3] B.-J. Kim, M.-L. Ha, Y.-S. Kwon, New through-wafer via interconnections with thick oxidized porous silicon sidewall via, Jpn. J. Appl. Phys. 45 (2006) 6141–6145.
[4] Cheryl S. Selvanayagam, John H. Lau, Xiaowu Zhang, S.K.W. Seah, Kripesh Vaidyanathan, T.C. Chai, Nonlinear thermal stress/strainanalysis of copper filled TSV (Through Silicon Via) and their Flip-chip microbumps, IEEE Trans. Adv. Packag. 32 (2009) 720–728.
[5] M. Motoyoshi, Through-Silicon Via (TSV), Proc. IEEE 97 (2009) 43–48.
[6] Y.-K. Ko, Y.-H. Ko, J.-H. Bang, C.-W. Lee, Technical trend of TSV (Through Silicon Via) filling for 3D wafer electric packaging, J. Weld. Join. 32 (2014) 19–26 (Korean).
[7] D.-G. Kim, J.-W. Kim, S.-S. Ha, J.-P. Jung, Y.-E. Shin, J.-H. Moon, S.-B. Jung, Fabrication of Through-hole interconnect in Si Wafer for 3D package, J. Weld. Join. 24 (2006) 64–70 (Korean).
[8] S. Sheng, A. Chandrakasan, R.W. Brodersen, A portable multimedia terminal, IEEE Commun. Mag. 30 (1992) 64–75.
[9] M. Karnezos, F. Carson, R. Pendse, Chip Scale Rev. 1 (2005) 29.
[10] M. Koyanagi, H. Kurino, K.W. Lee, K. Sakuma, N. Miyakawa, H. Itani, Future system-on-Silicon LSI chips, IEEE Micro 18 (1998) 17–22.
[11] K. Takahashi, M. Hoshino, H. Yonemura, M. Tomisaka, M. Sunohara, M. Tanioka, T. Sato, K. Kojima, H. Terao, Development of advanced 3D chip stacking technology with ultra-fine interconnection, in: Proceedings of the 51st Electron. Comp. Technol. Conf. , 2001, pp. 541–546.
[12] F.X. Che, W.N. Putra, A. Heryanto, Alastair Trigg, Xiaowu Zhang, C.L. Gan, Study on Cu protrusion of Through-silicon via, IEEE Trans. Comp. Pack. Man 3 (2013) 732–739.
[13] M.-H. Roh, A. Sharma, J.-H. Lee, J.-P. Jung, Extrusion suppression of TSV filling metal by Cu-W electroplating for three-dimensional microelectronic packaging, Metall. Mater. Trans. A 46A (2015) 2051–2062.
[14] Z. Wu, Z. Huang, Y. Ma, H. Xiong, P.P. Conway, Effects of the microstructure of copper Through-Silicon Vias on their thermally induced linear elastic mechanical behavior, Electron. Mater. Lett. 10 (2014) 281–292.
[15] T. Nakamura, H. Kitada, Y. Mizushima, N. Maeda, K. Fujimoto, T. Ohba, Comparative study of side-wall roughness effects on leakage currents in Through-Silicon Via interconnects, IEEE Int. 3D Syst. 2011 (2011) 2–4.
[16] J.C. Lin, W.C. Chiou, K.F. Yang, H.B. Chang, Y.C. Lin, E.B. Liao, J.P. Hung, Y.L. Lin, P.H. Tsai, Y.C. Shih, T.J. Wu, W.J. Wu, F.W. Tsai, Y.H. Huang, T.Y. Wang, C.L. Yu, C.H. Chang, M.F. Chen, S.Y. Hou, C.H. Tung, S.P. Jeng, Doug C.H. Yu, High density 3D integration using CMOS foundry technologies for 28 nm node and beyond, Intel. Devices Meet. 10 (2010) 2.1.1–2.1.4.
[17] J. Bea, K. Lee, T. Fukushima, T. Tanaka, M. Koyanagi, Evaluation of Cu diffusion from Cu Through-silicon via (TSV) in three-dimensional LSI by transient capacitance measurement, Electron. Devices Lett. 32 (2011) 940–942.
[18] K.-W. Lee, J.C. Bae, T. Fukushima, T. Tanaka, M. Koyanagi, Cu Retardation performance of extrinsic gettering layers in thinned wafers evaluated by transient capacitance measurement, J. Electrochem. Soc. 158 (2011) H795–H799.
[19] A.S. Budiman, H.A.S. Shin, B.J. Kim, S.H. Hwang, H.Y. Son, M.S. Suh, Q.H. Chung, K.Y. Byun, N. Tamura, M. Kunz, Y.C. Joo, Measurement of stresses in Cu and Si around Through-Silicon Via by synchrotron X-ray microdiffraction for 3-dimensional integrated circuits, Microelectron. Reliab. 52 (2012) 530–533.
[20] X. Liu, Q. Chen, V. Sundaram, R.R. Tummala, S.K. Sitaraman, Failure analysis of through-Silicon Vias in free-standing wafer, Microelectron. Reliab. 53 (2013) 70–78.
[21] S. Armini, Z. El-Mekki, K. Vandersmissen, H. Philipsen, S. Rodet, M. Honore, A. Radisic, Y. Civale, E. Beyne, L. Leunissen, Void-free filling of HAR TSVs using a wet alkaline Cu seed on CVD Co as a replacement for PVD Cu seed, J. Electrochem. Soc. 158 (2011) H160–H165.
[22] Y. Civale, S. Armini, H. Philipsen, A. Redolfi, D. Velenis, K. Croes, N. Heylen, Z. El-Mekki, K. Vandersmissen, G. Beyer, B. Swinnen, E. Beyne, Enhanced barrier seed metallization for high-density aspect-ratio copper-filled 3D Through-Silicon Via interconnects, in: Proceedings of the 62nd Elec. Comp. C IEEE, 2012, pp 822–826.
[23] D. Archard, K. Giles, A. Price, S. Burgess, K. Buchanan, Low temperature PECVD of dielectric films for TSV applications, in: Proceedings of the 60th Elec. Comp. C IEEE, 2010, pp. 764–768.
[24] N. Ranganathan, K. Prasad, N. Balasubramanian, K.L. Pey, A study of thermo-mechanical stress and its impact on Through-silicon vias, J. Micromech. Microeng. 18 (2008) 075018/1–075018/13.
[25] S.-K. Ryu, T. Jiang, K.H. Lu, J. Im, H.-Y. Son, K.-Y. Byun, R. Huang, P.S. Ho, Characterization of thermal stresses In Through-silicon vias for three-dimensional interconnects by bending beam technique, Appl. Phys. Lett. 100 (2012) 041901/1–041901/4.
[26] A. Heryanto, W.N. Putra, A. Trigg, S. Gao, W.S. Kwon, F.X. Che, X.F. Ang, J. Wei, R.I. Made, C.L. Gan, K.L. Pey, Effect of copper TSV annealing on via protrusion for TSV wafer fabrication, J. Electron. Mater. 41 (2012) 2533–2542.
[27] S.-K. Ryu, K.-H. Lu, J. Im, R. Huang, P.S. Ho, Stress-induced delamination of Through silicon via structures, AIP Conf. Proc. 1378 (2011) 153–167.
[28] M.-H. Liao, The special trench design Near the Through Silicon Vias (TSVs) to reduce the keep-out zone for application in three-dimensional integral circuits, J. Phys. D: Appl. Phys. 46 (2013) 495103/1–495103/5.
[29] B. Majeed, N.P. Pham, D.S. Tezcan, E. Beyne, Parylene N as a dielectric material for Through Silicon Vias, in: Proceedings of the 58th Electron. Comp. C IEEE, 2008, pp. 1556–1561.
[30] D.S. Tezcan, F. Duval, H. Philipsen, O. Luhn, P. Soussan, B. Swinnen, Scalable Through Silicon Via with polymer deep trench isolation for 3D wafer level packaging, in: Proceedings of the 59th Electreon. Comp. C IEEE, 2009, pp. 1159–1164.
[31] F.F.C. Duval, C. Okoro, Y. Civale, P. Soussan, E. Beyne, Polymer filling of silicon trenches for 3-D Through silicon vias applications, IEEE Trans. Comp. Pack. Man 1

(2011) 825–832.
[32] M. Wilke, F. Wippermann, K. Zoschke, M. Toepper, O. Ehrmann, H. Reichl, K.-D. Lang, Prospects and Limits in Wafer-Level-Packaging of Image Sensors, in: Proceedings of the 61st Electron. Comp. C IEEE, 2011, pp. 1901–1907.
[33] C. Truzzi, F. Raynal, V.M. Alchimer, Wet-process deposition of TSV liner and metal films, IEEE Int. 3D Syst. (2009) 1–6.
[34] S. Farrens, Evolution of bond technology to hybridized process flows, IEEE Int. 3D Syst. (2009) 1–4.
[35] R.K. Trichur, M. Fowler, J.W. McCutcheon, M. Daily, Filling and planarizing deep trenches with polymeric material for Through-Silicon Via technology, in: Proceedings IMAPS 3-D 6th Int. Conf. Exhibit. Dev. Package, 2010, pp. 192–195.
[36] J.-H. Im, E.O. Shaffer, T. Stokich, A. Strandjord, J. Hetzner, J. Curphy, C. Karas, G. Meyers, D. Hawn, A. Chakrabarti, S. Froelicher, On the mechanical reliability of photo-BCB-based thin film dielectric polymer for electronic packaging applications, J. Electron. Packag. 122 (2000) 28–33.
[37] Q. Chen, C. Huang, Z. Tan, Z. Wang, Low capacitance Through-silicon-vias with uniform benzocyclobutene insulation layers, IEEE Trans. Comp. Pack. Man 3 (2013) 724–731.
[38] M. Gonzalez, R. Labie, B. Vandevelde, E. Beyne, Proc. Pan Pacific Microelectron. Sym, 2005, pp. 9–14.
[39] B. Horváth, J. Kawakita, T. Chikyow, Through silicon via filling methods with metal/polymer composite for three-dimensional LSI, Jpn. J. Appl. Phys. 53 (2014) (06JH01/1-06JH01/5).
[40] Y.T. Ding, Y.Y. Yan, Q.W. Chen, S.W. Wang, X. Chen, Y.Y. Chen, Investigation on mechanism of polymer filling in high-aspect-ratio trenches for Through-Silicon-Via (TSV) application, Sci. China Tech. Sci. 57 (2014) 1616–1625.
[41] G. Decher, J.B. Schlenoff, Multilayer Thin Films, Wiley-VCH, Germany, 2002.
[42] Y. Okayama, T. Ito, S. Shiratori, Optimization of the feedback constant control for the mass-controlled layer-by-layer sequential adsorption technique for polyelectrolyte thin films, Thin Solid Films 393 (2001) 132–137.
[43] P.G. Ganesan, J. Gamba, A. Ellis, R.S. Kane, G. Ramanath, Polyelectrolyte nanolayers as diffusion barriers for Cu metallization, Appl. Phys. Lett. 83 (2003) 3302–3304.
[44] D.D. Gandhi, A.P. Singh, M. Lane, M. Eizenberg, G. Ramanath, Copper diffusion and mechanical toughness at Cu-silica interfaces glued with polyelectrolyte nanolayers, J. Appl. Phys. 101 (2007) 084505/1–084505/4.
[45] T.C. Wang, R.E. Cohen, M.F. Rubner, Metallodielectric photonic structures based on polyelectrolyte multilayers, Adv. Mater. 14 (2001) 1534–1537.
[46] M. Michel, V. Toniazzo, D. Ruch, V. Ball, Deposition mechanisms in layer-by-layer or step-by-step deposition methods: from elastic and impermeable films to soft membranes with ion exchange properties, ISRN Mater. Sci. 2012 (2012) 701695/1–701695/13.
[47] G. Ladam, P. Schaad, J.C. Voegel, P. Schaaf, G. Decher, F. Cuisinier, In situ determination of the structural properties of initially deposited polyelectrolyte multilayers, Langmuir 16 (2000) 1249–1255.
[48] D. Yoo, S.S. Shiratori, M.F. Rubner, Controlling bilayer composition and surface wettability of sequentially adsorbed multilayers of weak polyelectrolytes, Macromolecules 31 (1998) 4309–4318.
[49] M. Kolasińska, P. Warszyński, The effect of support material and conditioning on wettability of PAH/PSS multilayer films, Bioelectrochemistry 66 (2005) 65–70.
[50] W.C. Oliver, G.M. Pharr, An improved technique for determining hardness and elastic modulus using load and displacement sensing indentation experiments, J. Mater. Res. 7 (1992) 1564–1583.
[51] W. Martienssen, H. Warlimont, Handbook of Condensed Matter and Materials Data, Springer, Germany, 2005.
[52] J.D. Mendelsohn, C.J. Barrett, V.V. Chan, A.J. Pal, A.M. Mayes, M.F. Rubner, Fabrication of microporous thin films from polyelectrolyte multilayers, Langmuir 16 (2000) 5017–5023.
[53] S.S. Shiratori, M.F. Rubner, pH-dependent thickness behavior of sequentially adsorbed layers of weak polyelectrolytes, Macromolecules 33 (2000) 4213–4219.
[54] Y. Zhu, J. Shi, A mesoporous core-shell structure for pH-controlled storage and release of water-soluble drug, Microporous Mesoporous Mater. 103 (2007) 243–249.
[55] L. Dähne, G. Decher, J.B. Schlenoff (Eds.), Multilayer Thin Films, Wiley-VCH, Weinheim, 2003.
[56] Z. Liang, A. Susha, F. Caruso, Gold nanoparticle-based core-shell and hollow spheres and ordered assemblies thereof, Chem. Mater. 15 (2003) 3176–3183.
[57] B. Wu, A. Kumar, S. Pamarthy, High aspect ratio silicon etch: a review, J. Appl. Phys. 108 (2010) 051101/1–051101/20.
[58] G. Ramanath, G. Cui, P.G. Ganesan, X. Guo, A.V. Ellis, M. Stukowski, K. Vijayamohanan, P. Doppelt, M. Lane, Self-assembled subnanolayers as interfacial adhesion enhancers and diffusion barriers for integrated circuits, Appl. Phys. Lett. 83 (2003) 383–385.
[59] P.G. Ganesan, A.P. Singh, G. Ramanath, Diffusion barrier properties of carboxyl- and amine-terminated molecular nanolayers, Appl. Phys. Lett. 85 (2004) 579–581.
[60] D.D. Gandhi, U. Tisch, B. Singh, M. Eizenberg, G. Ramanath, Ultraviolet-oxidized mercaptan-terminated organosilane nanolayers as diffusion barriers at Cu-silica interfaces, Appl. Phys. Lett. 91 (2007) 143503/1–143503/3.
[61] E.M. Corcoron, Adhesion, Chapter 5.3, Paint Testing Manual, 13th ed., ASTM STP 500, ASTM, 1972, pp. 314–332.
[62] O.R. Rodriguez, W. Cho, R. Saxena, J.L. Plawsky, W.N. Gill, Mechanism of Cu diffusion in porous low- dielectrics, J. Appl. Phys. 98 (2005) 024108/1–024108/9.
[63] O.E. Rivera-Betancourt, E.S. Sheppard, D.C. Krause, R.A. Dluhy, Layer-by-layer polyelectrolyte encapsulation of mycoplasma pneumoniae for enhanced raman detection, Analyst 139 (2014) 4287–4295.
[64] H. Li, J.J. Vlassak, Determining the elastic modulus and hardness of an ultra-thin film on a substrate using nanoindentation, J. Mater. Res. 24 (2009) 1114–1126.
[65] R. Saha, Z. Xue, Y. Huang, W.D. Nix, Indentation of a soft metal film on a hard substrate: strain gradient hardening effects, J. Mech. Phys. Solids 49 (2001) 1997–2014.
[66] R. Saha, W.D. Nix, Effects of the substrate on the determination of thin film mechanical properties by nanoindentation, Acta Mater. 50 (2002) 23–38.
[67] Z. Wang, A.A. Volinsky, N.D. Gallant, Nanoindentation study of polydimethylsiloxane elastic modulus using Berkovich and flat punch tips, J. Appl. Polym. Sci. 132 (2015) 41384/1–41384/7.
[68] F.D. Paoli, Measuring Polydimethylsiloxane (PDMS) Mechanical Properties Using Flat Punch Nanoindentation Focusing on Obtaining Full Contact, (2015), pp. 32–34.
[69] R.B. King, Elastic analysis of some punch problems for a layered medium, Int. J. Solids Struct. 23 (1987) 1657–1664.